TSINGHUA SCIENCE AND TECHNOLOGY
ISSN 1007-0214
DOI: 10.26599/TST.2025.9010145

Research Article

Machine Learning-Based Remote Sensing Retrieval of Nutrient Concentrations in China's Coastal Waters

Zhuoqi Zheng, Delu Pan, Zhenke Zhang, Difeng Wang*, Fang Gong, Jingjing Huang, Xianqiang He, Qing Zhang, and Aifen Zhong

Abstract: Dissolved inorganic nitrogen (DIN) and dissolved inorganic phosphorus (DIP) are the two dominant nutrients influencing seawater quality. Due to the non-optically active nature of nutrients and their regional variability, relying solely on optical data is inadequate for achieving high-precision remote sensing retrieval in complex marine environments. We developed a novel remote sensing algorithm for DIN and DIP using MODIS remote sensing reflectance (Rrs) products and the XGBoost machine learning framework. Beyond optical inputs, our model integrates sea surface temperature (SST) and spatiotemporal information, including a shoreline-based pixel location descriptor, which significantly enhances model performance. We generated monthly average distributions of DIN and DIP concentrations across China's coastal waters from 2012 to 2022. The findings highlight extensive high-nutrient zones in the Bohai Bay and Changjiang River (Yangtze River) Estuary−Hangzhou Bay regions, with a notable declining trend in nutrient concentrations. The Zhujiang River (Pearl River) Estuary also exhibits elevated nutrient levels, albeit with minimal changes. This study pioneers the incorporation of dual-coordinate information in nutrient retrieval for complex marine environments, significantly improving model accuracy and addressing stripping artifacts associated with single-coordinate systems. Moreover, the results provide unprecedented spatiotemporal insights into nutrient distributions in China's coastal waters, offering valuable support for marine environmental management and policy-making.

Key words: dissolved inorganic nitrogen; dissolved inorganic phosphorus; machine learning; marine water quality

1 Introduction

Nutrients in seawater play a vital role in marine ecosystems, providing the essential material basis for the survival and reproduction of marine life. Nitrogen and phosphorus are introduced into coastal waters through various pathways, including terrestrial runoff, atmospheric deposition, and sediment diffusion[1–3]. However, an overabundance of these nutrients can trigger eutrophication, harmful algal blooms, and red tides, posing significant threats to marine ecosystems[4–7]. Historical data from the Report on the State of the Ecology and Environment in China consistently highlight that elevated levels of inorganic

• Zhuoqi Zheng is with School of Geography and Ocean Science, Nanjing University, Nanjing 210023, China, and also with the Second Institute of Oceanography, Ministry of Natural Resources, Hangzhou 310012, China. E-mail: zzq@sio.org.cn.
• Delu Pan, Jingjing Huang, Xianqiang He, Qing Zhang, and Aifen Zhong are with the Second Institute of Oceanography, Ministry of Natural Resources, Hangzhou 310012, China. E-mail: pandelu@sio.org.cn; leowatson@sio.org.cn; hexianqiang@sio.org.cn; zhangqing22@sio.org.cn; faizhobg@163.com.
• Zhenke Zhang is with the School of Geography and Ocean Science, Nanjing University, Nanjing 210023, China. E-mail: zhangzk@nju.edu.cn.
• Difeng Wang and Fang Gong are also with the Second Institute of Oceanography, Ministry of Natural Resources, Hangzhou 310012, China, and also with the Observation and Research Station for Marine Risk and Hazard Management at Daya Bay, Ministry of Natural Resources, Huizhou 516081, China. E-mail: dfwang@sio.org.cn; gongfang@sio.org.cn.
* To whom correspondence should be addressed.
Manuscript received: 2025-04-10; revised: 2025-07-27; accepted: 2025-09-10

nitrogen and active phosphate are key contributors to the decline in seawater quality along China's coast. Consequently, precise and comprehensive monitoring of nitrogen and phosphorus concentrations is essential for effective water quality management and environmental protection.

Satellite remote sensing provides a more extensive and temporally continuous perspective, addressing the spatial and temporal blind spots inherent in traditional seawater nutrient monitoring methods. Conventional techniques for retrieving nitrogen and phosphorus concentrations, such as least squares regression[8], multiple linear regression[9], and principal component regression[10], have been widely used. However, the retrieval accuracy of dissolved inorganic nitrogen (DIN) and dissolved inorganic phosphorus (DIP) remains limited because these nutrients are non-optically active, unlike other water quality parameters such as chlorophyll-*a* (CHL) and total suspended solids (TSS). In recent years, researchers have turned to neural networks for nutrient retrieval, demonstrating significant success in diverse environments, including lakes[11, 12], estuaries[13, 14], and bays[15, 16]. Despite these advancements, most studies have focused on small-scale regions or global-scale analyses, leaving a notable gap in large-scale, nationwide nutrient retrieval research. This limitation underscores the need for innovative approaches to address the regional variability and complexity of nutrient distributions across broader spatial extents. Furthermore, as machine learning algorithms are increasingly applied to remote sensing retrieval, investigating their convergence rate, generalizability, and stability remains a significant challenge[17]. Regarding the convergence rate, researchers introduce gradient-based differential neural-solution, which achieves a super-fast convergence and greatly promotes the development of the field[18]. Another breakthrough is for the generalization and stability of machine learning training, which are significantly enhanced by introducing an efficient new perspective and subtly applying special activation functions to gradients[19]. However, these methods may not be well suited to the field of remote sensing.

This study leverages publicly accessible water quality datasets from China's coastal waters and MODIS Level 2 (L2) products to retrieve DIN and DIP concentrations using the extreme gradient boosting (XGBoost) algorithm. A key innovation in our model is the integration of shoreline information, which substantially improves retrieval accuracy. After conducting quality control and data screening on the *in situ* DIN and DIP, we performed pixel matching between the *in situ* data (based on their measured latitudes and longitudes) and the monthly-averaged remote sensing data. The corresponding ocean color (OC) data, sea surface temperature (SST), and spatiotemporal information (STI) data were used as inputs to the XGBoost model, while the *in situ* DIN and DIP served as the outputs to construct the retrieval model. After selecting the optimal model, we applied it to the remote sensing data to generate monthly nutrient concentration products. Missing values were filled using the DINEOF method. We analyze the spatial and temporal dynamics of DIN and DIP across China's coastal waters from 2012 to 2022 and investigate the mechanisms influencing these patterns. The comprehensive research framework is depicted in Fig. 1. All abbreviations used in this paper and their meanings are listed in Table 1.

2 Data and method

2.1 Study area

China's coastal waters, stretching from north to south, comprise the Bohai Sea, Yellow Sea, East China Sea, and South China Sea (Fig. 2). Based on the distribution of *in situ* data, this study focuses on the maritime region within 16°N–41°N and 107°E–127°E. Additionally, three key sub-regions were selected as primary high-nutrient zones in China's coastal waters:

- **Region A (Bohai Sea):** This area includes the estuaries of several major rivers, notably the Yellow River, one of China's two largest rivers.
- **Region B (East China Sea):** This region encompasses the Changjiang River (Yangtze River) Estuary, the other of China's two largest rivers.
- **Region C (South China Sea):** This area features the Zhujiang River (Pearl River) Estuary, another significant source of nutrient input.

These sub-regions were chosen due to their high nutrient concentrations and ecological significance, driven by substantial riverine discharges and anthropogenic influences.

2.2 Data

2.2.1 *In situ* data

The *in situ* data used in this study comprise a

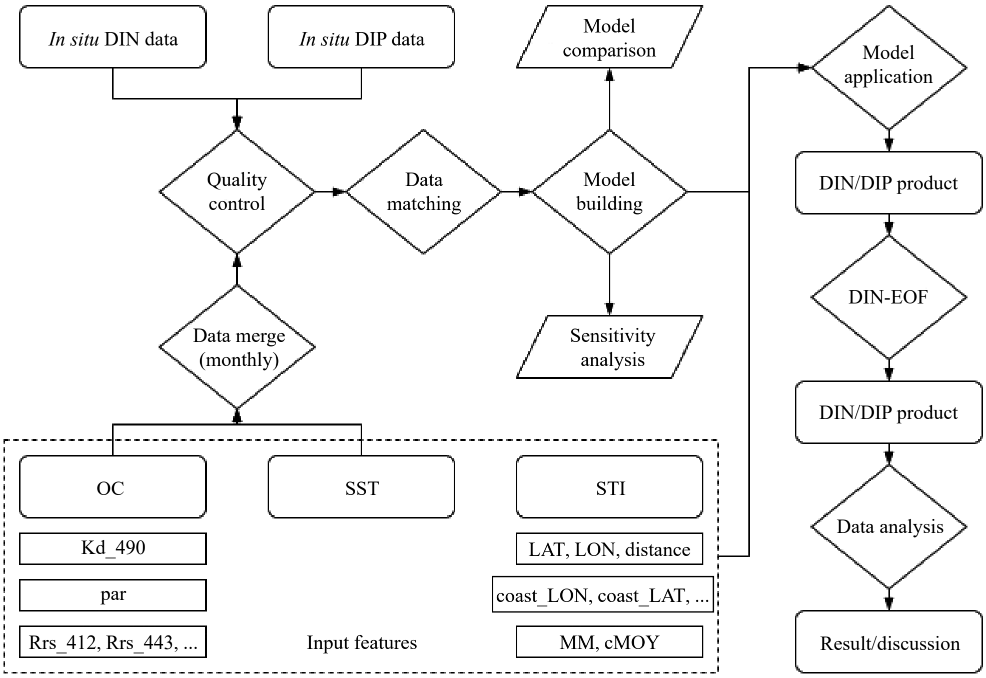

Fig. 1 Flowchart of this study. Based on *in situ* measured DIN and DIP data as well as MODIS data, a remote sensing retrieval algorithm for nutrients in the study area was constructed, and the long-term time-series results of remotely sensed nutrients were analyzed and discussed.

comprehensive water quality parameter dataset for China's jurisdictional waters from 2012 to 2022[20]. This dataset was curated by Lin et al.[20], who collected, organized, restructured, and compiled publicly available data from the National Marine Environmental Monitoring Center (NMEMC) using R and Python programming languages. Monthly coastal and marine water quality data are accessible via the NMEMC platform (http://ep.nmemc.org.cn:8888/Water/). The observational data provide monthly measurements of coastal and marine water quality parameters.

2.2.2 Remote sensing data

For this study, MODIS L2 products were utilized to investigate nutrient concentrations. Daily OC and SST products at MODIS L2A level were obtained from the OceanColor website (https://oceancolor.gsfc.nasa.gov/) for the period 2012–2022. The spatial extent is limited to 16°N–41°N and 107°E–127°E, with a spatial resolution of 1 km.

2.2.3 Elevation and bathymetric data

The GEBCO_2024 grid[21] is a global terrain model for both ocean and land, providing elevation data at a 15-arc-second interval grid resolution, with values expressed in meters. In this study, the elevation and bathymetric data from GEBCO_2024 were used as the standard for delineating the study area. The dataset is accessible via https://doi:10.5285/1c44ce99-0a0d-5f4f-e063-7086abc0ea0f.

2.2.4 Climate data

The Niño 3.4 index is the most commonly used metric for defining El Niño and La Niña events. The Niño 3.4 anomaly represents the average SST across the equatorial Pacific Ocean, spanning from the international date line to the coast of South America. The Niño 3.4 index is typically calculated using a 5-month running mean, and an El Niño or La Niña event is identified when the Niño 3.4 SST anomaly exceeds ±0.4°C for a period of six months or longer. The Niño 3.4 data used in this study were obtained from https://psl.noaa.gov/data/correlation/nina34.data.

Monthly precipitation data[22] for China from 1901 to 2023, with a spatial resolution of 0.008 333 3° (approximately 1 km), were utilized in this study. This dataset, representing monthly precipitation across China, was generated using the Delta spatial downscaling method, based on the global 0.5° climate dataset released by the climatic research unit (CRU) and the high-resolution global climate dataset from WorldClim. The downscaled data were validated using observations from 496 independent meteorological stations, demonstrating high reliability. The dataset is

Table 1 List of abbreviations.

Abbreviation	Full term
BPNN	Backpropagation neural network
CHL	Chlorophyll-*a*
CMEMS	Copernicus Marine Environment Monitoring Service
CNN	Convolutional neural network
CRU	Climatic research unit
DIN	Dissolved inorganic nitrogen
DINEOF	Data interpolating empirical orthogonal functions
DIP	Dissolved inorganic phosphorus
DNB	Day/night band
Kd_490	Diffuse attenuation coefficient at 490 nm
L2	Level 2
MAE	Mean absolute error
MAPE	Mean absolute percentage error
MM	Two-character month representation
cMOY	Cyclic month of year
NMEMC	National Marine Environmental Monitoring Center
OC	Ocean color
par	Photosynthetically active radiation
R^2	Coefficient of determination
RF	Random forest
RMSE	Root mean square error
Rrs_λ	Remote sensing reflectance at wavelength λ (nm)
SNPP	Suomi National Polar-orbiting Partnership
SST	Sea surface temperature
STI	Spatiotemporal information
TSS	Total suspended solids
VC	Variation coefficient
VIIRS	Visible infrared imaging radiometer suite
XGBoost	Extreme gradient boosting

accessible via https://doi.org/10.5281/zenodo.3114194.

2.2.5 Nighttime light data

Nighttime light data were obtained from the Suomi National Polar-orbiting Partnership (SNPP) satellite, launched in 2011. The satellite's Visible Infrared Imaging Radiometer Suite (VIIRS) captures nighttime light imagery through the day/night band (DNB), with a typical resolution of 500 m. These data are accessible via https://eogdata.mines.edu/products/vnl/.

2.3 Methodology

2.3.1 Nutrient retrieval model development

XGBoost is a powerful machine learning tool, fundamentally a tree-boosting algorithm widely applied in retrieval algorithms due to its efficiency and versatility[23]. It demonstrates exceptional performance in scenarios with limited training data. In preliminary experiments, we found that XGBoost outperformed other methods, such as random forest (RF) and convolutional neural network (CNN), in terms of training efficiency and accuracy.

2.3.2 Data matching

Since the publicly available *in situ* data are provided as monthly averages, we calculated monthly averages of the remote sensing data to ensure temporal consistency. To maintain data quality, the following steps were applied to filter the monthly averaged data:

● For each *in situ* data station, to reduce spatial misalignment, suppress noise, and improve representativeness[24, 25], all pixels within a 3 × 3 grid

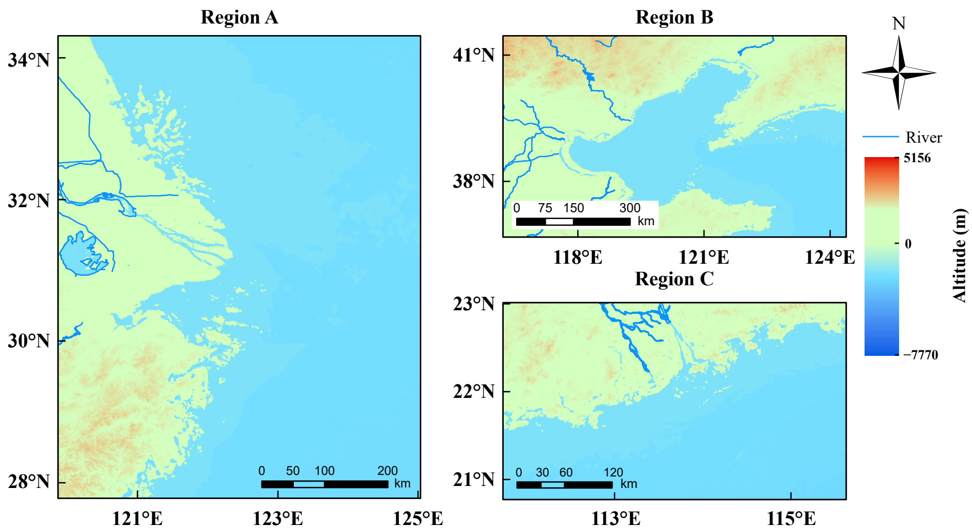

Fig. 2 Study area and key sub-regions. Region A is defined by coordinates 37°N–41°N and 117°E–123°E, Region B spans 28°N–34°N and 120°E–125°E, and Region C covers 21°N–23°N and 112°E–115°E, with bathymetric data sourced from the GEBCO_2024 dataset.

centered on the corresponding latitude and longitude were extracted from the monthly remote sensing data.

- The variation coefficient (VC, calculated as standard deviation (SD)/mean) was computed for each group of pixels, ensuring it remained within 15%. If the VC exceeded 15%, the pixel with the highest standard deviation was iteratively removed until the criterion was met.
- The average value of the remaining pixels was calculated and used as the matched result for the corresponding *in situ* station.

2.3.3 Accuracy assessment and sensitivity analysis

In this study, we used the coefficient of determination (R^2), root mean square error (RMSE), mean absolute error (MAE), and mean absolute percentage error (MAPE) as evaluation metrics for nutrient modeling. To investigate the influence of various factors on the model, correlation analysis and local sensitivity analysis were employed. Correlation analysis involves calculating the correlation coefficient (r) between each factor and nutrient concentrations. Local sensitivity analysis evaluates the impact of individual features on model predictions by varying their values and observing changes in the model output (i.e., RMSE). This method is particularly useful for understanding the contribution of individual features to model performance. The expressions for the aforementioned parameters are as follows:

$$r = \frac{\sum_{i=1}^{n}(a_i - \overline{a})(b_i - \overline{b})}{\sqrt{\sum_{i=1}^{n}(a_i - \overline{a})^2 \sum_{i=1}^{n}(b_i - \overline{b})^2}} \tag{1}$$

$$R^2 = 1 - \frac{\sum_{i=1}^{n}(y_i - \hat{y}_i)^2}{\sum_{i=1}^{n}(y_i - \overline{y})^2} \tag{2}$$

$$\text{RMSE} = \sqrt{\frac{1}{n}\sum_{i=1}^{n}(y_i - \hat{y}_i)^2} \tag{3}$$

$$\text{MAE} = \frac{1}{n}\sum_{i=1}^{n}|y_i - \hat{y}_i| \tag{4}$$

$$\text{MAPE} = \frac{1}{n}\sum_{i=1}^{n}\left|\frac{y_i - \hat{y}_i}{y_i}\right| \times 100\% \tag{5}$$

where a_i and b_i are the i-th elements of two sample sequences each of length n, and $\bar{a}$ and $\bar{b}$ are the sample means of the two sequences, respectively. y_i is the actual value of the i-th sample; $\hat{y}_i$ is the predicted value of the i-th sample; $\overline{y}$ is the mean of the actual values across all samples; and n is the total number of samples.

3 Result

3.1 Distribution of *in situ* data

We analyzed the spatial and temporal distribution of the *in situ* data (Table 2). Temporally, monitoring was primarily conducted during spring (April–June), summer (July–September), and autumn (October–December), with no water quality measurements taken during winter. Within these seasons, sampling was concentrated in May, August, and October. This sampling strategy offers strong stability, enabling accurate year-on-year and month-on-month comparisons of parameters. However, it may overlook monthly variations in nutrient concentrations.

The distribution of *in situ* data sampling points is shown in Fig. 3. Spatially, the sampling strategy clearly prioritizes nearshore areas, with sampling points densely distributed along the coastline. A limited number of offshore sampling points are observed during summer, likely due to maritime conditions and safety management policies. Additionally, a significant proportion of sampling points are located at the estuaries of major rivers, such as the Zhujiang River, Yellow River, and Changjiang River.

3.2 Nutrient model development results

During model development, we incorporated Ocean color parameters, SST, and STI (Table 3). Among

Table 2 Total monthly *in situ* data volume.

Month	Number of data
January	0
February	0
March	0
April	2160
May	4267
June	112
July	3072
August	4231
September	216
October	4117
November	1149
December	45

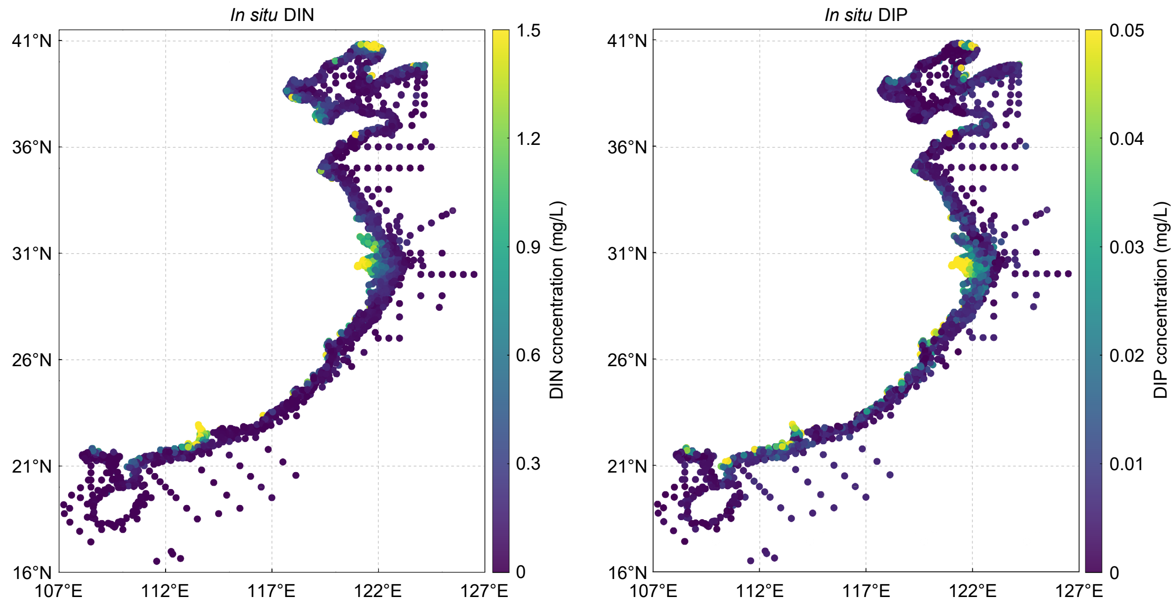

Fig. 3 Distributions of sampling points for *in situ* nutrient concentrations data. The color of each sampling point indicates the magnitude of the measured nutrient concentration, as shown in the colorbar on the right.

Table 3 Input parameters.

Parameter category	Model parameter
OC	Kd_490, Rrs_412, Rrs_443, Rrs_469, Rrs_488, Rrs_531, Rrs_547, Rrs_555, Rrs_645, Rrs_667, Rrs_678, par
SST	SST
STI	LON, LAT, distance, coast_LON, coast_LAT, coast_ID, MM, cMOY

these, cMOY represents the cyclic month of year, which captures the cyclical variation of months across years, expressed as

$$\text{cMOY} = 1 - \cos\left(\frac{\text{MM}}{12} \times 2\pi\right) \tag{6}$$

For spatial information, we introduced a set of parameters to describe the pixel's position relative to the coastline, including the distance to the coastline, the latitude and longitude coordinates of the nearest coastal point, and a segment index. The coastline data were derived from a shapefile (shp) of China's land boundaries provided by the Ministry of Natural Resources. After removing all islands and retaining only the mainland, the coastline was defined by 257 779 vertices. Starting from the northernmost point, each vertex was sequentially numbered clockwise to create a segment index for the coastline. These parameters include coast_LON, coast_LAT, distance, and coast_ID. distance denotes the shortest geographic distance from the *in situ* measurement point to the projected point on the nearest coastline, in unit of km, quantifying the potential influence of terrestrial input on the sample point. coast_LON and coast_LAT represent the longitude and latitude of this nearest projected point, respectively. coast_ID is used to identify between which two adjacent nodes in the coastline vector data the projected point is located, thereby providing index information for the continuity of nearshore spatial relationships.

In this model development experiment, we simultaneously trained and evaluated XGBoost, RF, backpropagation neural networks (BPNNs), and CNNs (Table 4). To ensure a fair comparison, all models were trained with the same number of iterations and parameter optimization strategies. Through systematic performance evaluation, the XGBoost model demonstrated significant advantages across multiple key metrics. Additionally, we found that, overall, tree-based models outperformed neural networks in nutrient retrieval, confirming the superior performance of decision tree-based methods in addressing nutrient retrieval problems and highlighting their robust capability in handling complex nonlinear relationships.

After data matching and filtering out invalid or missing values, we obtained 2882 matched data points. These 2882 data points, along with their 21 input parameters, were used to train the XGBoost model. The dataset was randomly split into a training set (70%) and a validation set (30%). We employed five-

Table 4 Performance comparison of different neural network models for remote sensing retrieval of DIN and DIP concentrations.

Metric	Metric value							
	DIN concentration				DIP concentration			
	XGBoost	RF	CNN	BPNN	XGBoost	RF	CNN	BPNN
R^2	0.55	0.42	0.41	0.35	0.29	0.28	0.20	0.13
RMSE (mg/L)	0.15	0.17	0.17	0.18	0.011	0.011	0.011	0.012
MAE (mg/L)	0.095	0.10	0.11	0.11	0.0060	0.0060	0.0065	0.0068
MAPE (%)	119.6	163.2	150.4	171.8	120.1	122.7	139.4	143.1
p	<0.05	<0.05	<0.05	<0.05	<0.05	<0.05	<0.05	<0.05

fold cross-validation to evaluate the model's performance, with RMSE as the primary metric. The model was trained to retrieve DIN and DIP concentrations, and the results are visualized in scatter plots shown in Fig. 4. Overall, the retrieval performance for DIN was satisfactory, with R^2 exceeding 0.80 and RMSE values remaining below 0.10 mg/L in both the training and validation datasets. In contrast, the model performance for DIP was comparatively limited, yielding an R^2 of 0.65 for the training set and 0.70 for the validation set, with RMSE values consistently around 0.006 mg/L. This discrepancy may be attributed to the inherently low concentration levels of DIP and its narrow dynamic

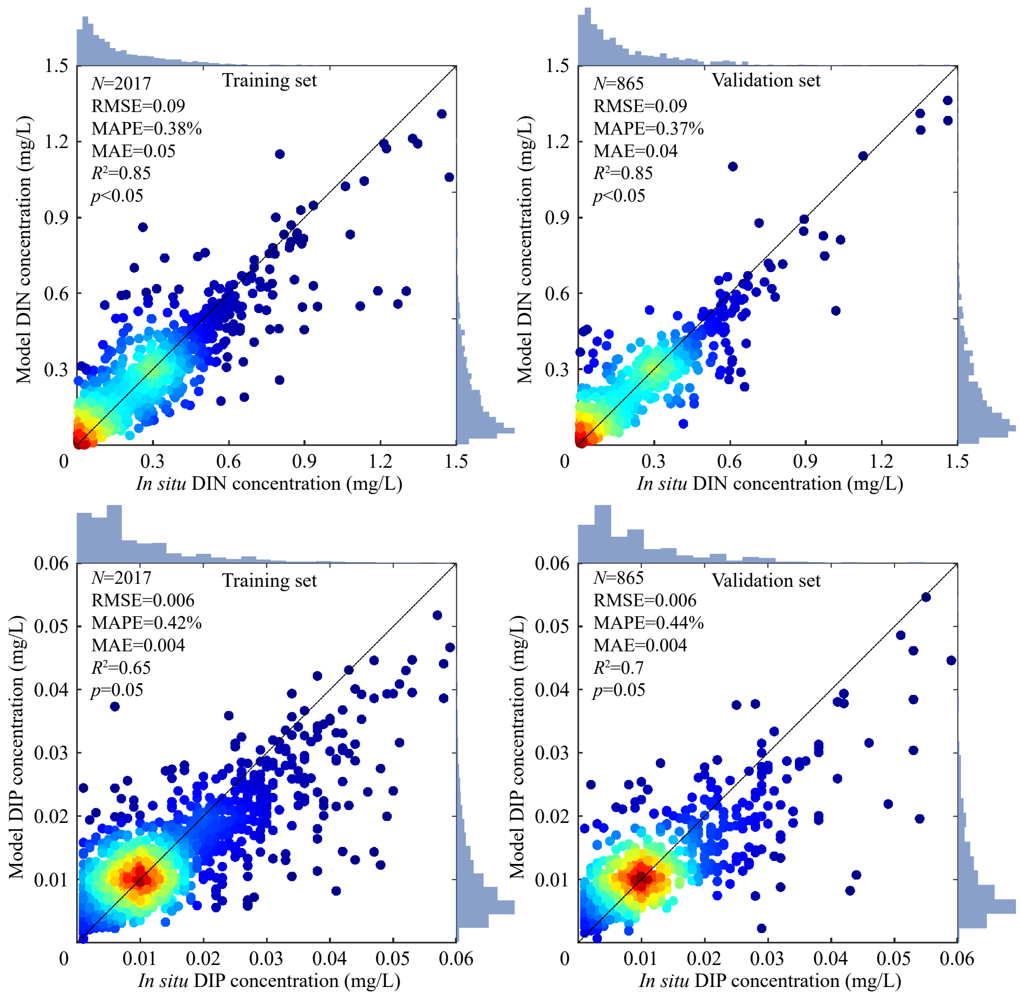

Fig. 4 Results for the training and validation sets of DIN and DIP concentrations shown in scatter plots. The color of the scatter points represents their density, with a gradient from blue to red indicating increasing point density within each interval. Histograms adjacent to the axes display the number of scatter points within each interval.

range, which constrain the model's ability to capture variability effectively.

3.3 Spatiotemporal distribution of nutrient retrieval results

The MODIS L2A products from 2012 to 2022 were resampled to a 0.01° resolution and aggregated into monthly averages. A predefined 2501 × 2001 grid, covering a geographical range of 16°N–41°N and 107°E–127°E with a resolution of 0.01°, was used. For each MODIS parameter, all monthly data were interpolated using cubic interpolation based on triangulation to generate monthly averaged parameter products. These monthly products were then used as inputs for the model to produce corresponding monthly averaged nutrient concentration products.

After generating the monthly nutrient products, missing data were filled using the Data Interpolating Empirical Orthogonal Functions (DINEOF) method[26, 27], resulting in gap-free monthly averaged DIN and DIP concentrations products for 2012–2022. Since coastal water quality parameters are significantly influenced by human activities and terrestrial runoff, only data within 200 nautical miles offshore and at depths less than 200 m were analyzed. Figures 5 and 6 show the climatological monthly averaged nutrient concentrations, revealing distinct regional patterns. High nutrient concentrations were primarily observed in the Liaodong Bay, Bohai Bay, Laizhou Bay, Hangzhou Bay, Daya Bay (Zhujiang River Estuary), and Beibu Gulf, all of which are estuaries of major rivers. Temporally, nutrient concentrations in the Bohai Sea, Yellow Sea, and East China Sea exhibited a winter-high and summer-low pattern, while the South China Sea showed a summer-high and winter-low pattern.

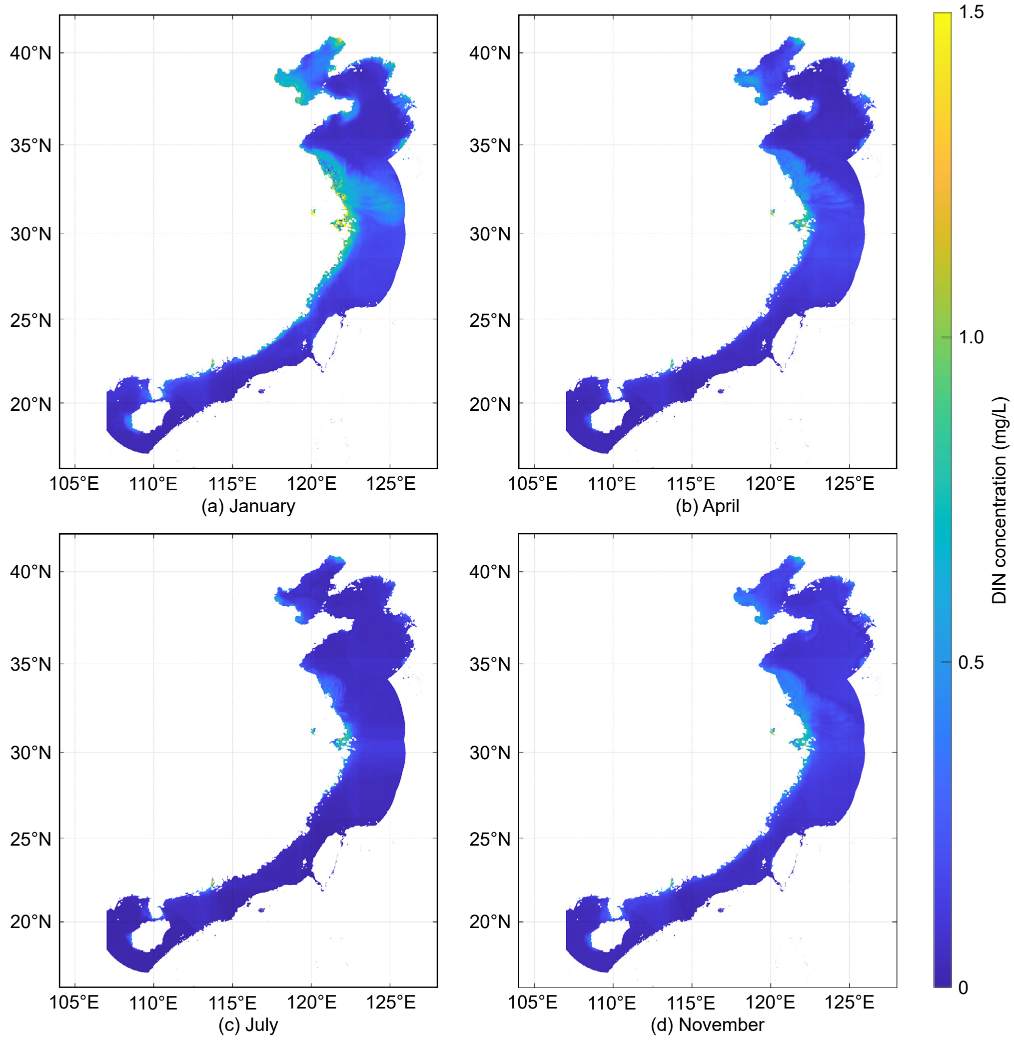

Fig. 5 Climatological monthly averages of DIN concentration. (a) January, (b) April, (c) July, and (d) November.

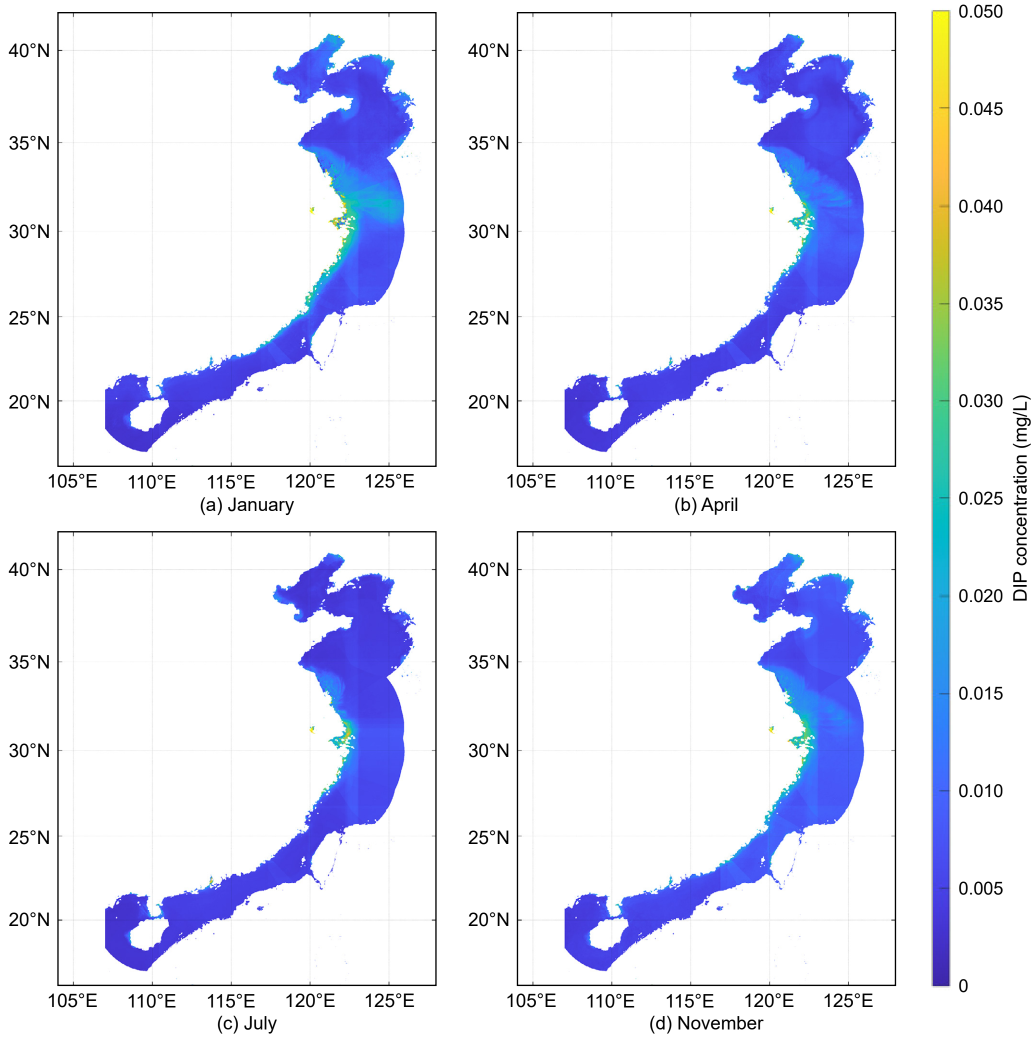

Fig. 6 Climatological monthly averages of DIP concentration. (a) January, (b) April, (c) July, and (d) November.

According to the nutrient concentration distribution derived from our model, the spatial patterns of high-nutrient regions are consistent with those reported in the Report on the State of the Ecology and Environment in China. The report highlights three key marine areas with serious nutrient enrichment issues, which precisely coincide with the three major regions targeted in our study: The Bohai Sea, the Changjiang River Estuary–Hangzhou Bay, and the Zhujiang River Estuary. Other high-nutrient zones identified in our results, such as the Liaodong Bay and the northern Yellow Sea, also align with the areas emphasized in the report.

In terms of temporal distribution, the report indicates that nutrient concentrations in China's coastal waters are lower in summer compared to spring and autumn—an observation that is also reflected in our findings. Previous studies by Wu et al.[15] and Zhu et al.[13], which focused on nutrient retrieval using remote sensing in the coastal waters of Zhejiang Province and Guangdong Province, respectively, have provided more detailed regional insights. The spatial and temporal patterns observed in our results for the Changjiang River Estuary–Hangzhou Bay and the Zhujiang River Estuary are in good agreement with their findings, further demonstrating the reliability and reference value of our research.

3.4 Long-term trends in nutrient retrieval results

By averaging the monthly nutrient concentration products, the long-term trends in nutrient levels in China's coastal waters from 2012 to 2022 were plotted (Fig. 7). The overall nutrient concentrations exhibited cyclical variations. Generally, nutrient levels in the Bohai Bay and Changjiang River Estuary–Hangzhou Bay regions were higher than those in the Zhujiang

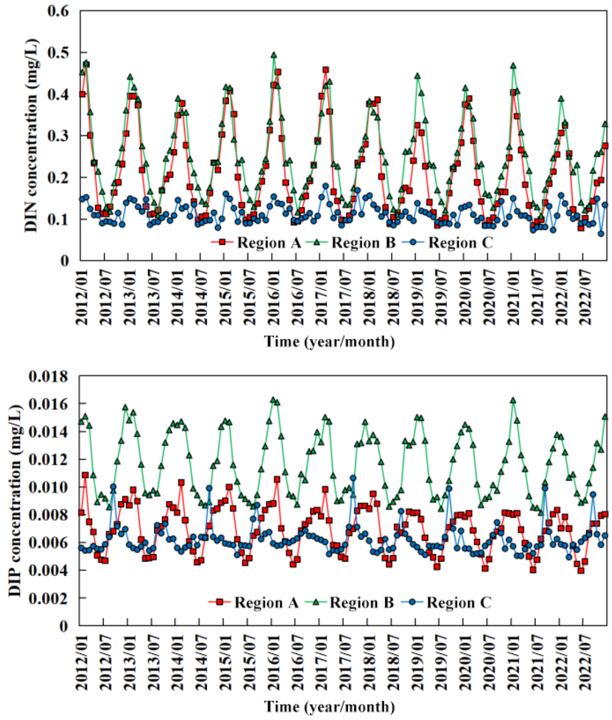

Fig. 7 Monthly trends in nutrient concentrations in the three key sub-regions.

River Estuary. Both the Bohai Bay and Changjiang River Estuary–Hangzhou Bay regions showed similar seasonal trends, with higher nutrient levels in winter and lower levels in summer. In the Bohai Bay, this pattern is largely driven by nutrient inputs from the Yellow River, making nutrient concentrations in this region a reflection of the river's discharge. In the Changjiang River Estuary–Hangzhou Bay region, the mixing of Changjiang River water with intruding offshore seawater during summer causes a significant dilution effect. In winter, stronger vertical mixing due to lower temperatures allows seawater to intrude further onto the shelf, raising nutrient levels across the region. In contrast, the Zhujiang River Estuary exhibits a different trend, characterized by a sudden decline in DIN concentration levels during October to November. Additionally, the DIP trend in the Zhujiang River Estuary is opposite to that in the Bohai Bay and Changjiang River Estuary–Hangzhou Bay regions, with lower levels in spring and winter and higher concentration levels in summer and autumn.

4 Discussion

4.1 Impact of input features on the nutrient model

During model development, we experimented with different combinations of input features, including OC, SST, STI, and shoreline information. Compared to using only OC and SST data, the addition of STI significantly improved model accuracy, substantially increasing R^2 and reducing RMSE. Further incorporating shoreline information enhanced model performance even more. This is because shoreline information provides an additional coordinate system for describing geographic locations, addressing the limitations of relying solely on latitude and longitude for spatiotemporal distribution in large-scale marine areas. Without this, the retrieval results often exhibit horizontal and vertical striping artifacts. The inclusion of an alternative spatial coordinate system mitigates these artifacts to some extent (Table 5).

Additionally, we conducted correlation analysis and local sensitivity analysis for all input features (Fig. 8). Correlation analysis involved calculating the correlation coefficients between each input feature and DIN/DIP concentrations, while local sensitivity analysis evaluated the impact of individual features on model predictions by varying their values and observing changes in RMSE. This method is particularly useful for understanding the influence of individual features on model performance. For ocean color parameters, Rrs_645, Rrs_667, and Rrs_678 showed strong correlations with both nutrients, while shorter wavelengths exhibited weaker correlations. The 667 nm band demonstrated high sensitivity in modeling both DIN and DIP, making it a key band for nutrient retrieval, whereas the 678 nm band showed lower

Table 5 Performance comparison of different input parameter combinations for remote sensing retrieval of DIN and DIP concentrations.

Input feature	DIN concentration				DIP concentration			
	Training		Test		Training		Test	
	RMSE (mg/L)	R^2	RMSE (mg/L)	R^2	RMSE (mg/L)	R^2	RMSE (mg/L)	R^2
OC+SST	0.170	0.47	0.201	0.20	0.011	0.31	0.013	0.10
OC+SST+STI	0.061	0.93	0.168	0.48	0.0069	0.72	0.012	0.21
OC+SST+STI+coast	0.060	0.93	0.166	0.49	0.0051	0.82	0.012	0.26

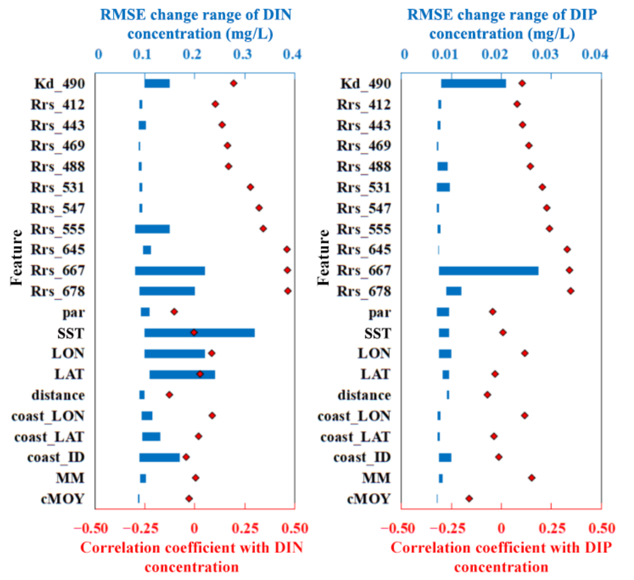

Fig. 8 Results of sensitivity analysis and correlation analysis for input features. The blue bars represent the range of changes in model performance (in terms of RMSE) caused by varying the values of different input features, while the red diamonds indicate the correlation coefficient between each input feature and nutrient concentrations.

sensitivity for DIP. Kd_490 performed well in the sensitivity analysis for DIP. Latitude and longitude showed better sensitivity results for DIN than for DIP, with latitude slightly outperforming longitude in both correlation and sensitivity analyses, likely due to the predominantly north-south orientation of the coastline. Among shoreline features, the input parameter coast_ID performed well, highlighting the characteristic distribution of nutrients along the coastline.

We also conducted global sensitivity analysis on the input features. The impact of removing each feature from the original model on the evaluation metric (RMSE) was assessed individually. Figure 9 shows the global sensitivity analysis results for DIN modeling. Removing most features increased the RMSE, indicating a degradation in model performance. For some features, such as Rrs_412, Rrs_488, Rrs_531, and Rrs_555, removing them caused a slight decrease or increase in RMSE, suggesting their influence on model performance is limited. However, removing SST and coast_LON reduced the RMSE, implying an improvement in model performance. For SST, its distribution trend in coastal waters is weakly correlated with nutrient concentrations, and it has no significant impact on nutrient distribution mechanisms at the mesoscale. Nevertheless, as an important indicator of marine environmental conditions, we believe it should be retained. For coast_LON, China's coastline is predominantly north-south oriented, with limited east-west distribution except in regions like Guangdong Province, parts of the Bohai Bay, and a few other areas. Thus, its correlation with overall nutrient distribution is very low. However, as a descriptor of spatial information, we consider it worth retaining.

Based on the above analysis, we have drawn the following preliminary conclusions regarding the influence of various features on nutrient retrieval results. The overall impact can be likened to the superposition of high-frequency and low-frequency information. High-frequency information, provided by remote sensing-derived OC and SST data, captures instantaneous changes in nutrient concentrations. In contrast, spatiotemporal information provides low-frequency information, reflecting the fundamental patterns of nutrient distribution under climatological or long-term conditions. For spatial information, we found that using a single coordinate system introduces striping artifacts in the retrieval results. To mitigate this, we introduced a dual-coordinate system, combining latitude/longitude and shoreline information, to reduce the overemphasis on low-frequency information from a single coordinate system. Given the strong regional characteristics of nutrient distribution, spatiotemporal information, which describes spatial variations, contributes significantly to mesoscale nutrient retrieval. Among OC features, longer wavelength bands appear to be more beneficial for nutrient modeling. We hypothesize that this is because longer wavelengths exhibit strong correlations with various ocean color parameters, such as suspended particulate matter, which share similar distribution patterns with nutrients, thereby enhancing model performance.

In the field of machine learning modeling for remote sensing retrieval of optically inactive marine parameters, the incorporation of spatiotemporal information as input has emerged as a novel research direction. In several regional-scale case studies, the addition of latitude, longitude, and temporal features has been shown to significantly improve retrieval accuracy. Spatiotemporal information can partially reflect the regional characteristics of marine parameters and serves as a bridge linking the spatial relationships among different remote sensing pixels.

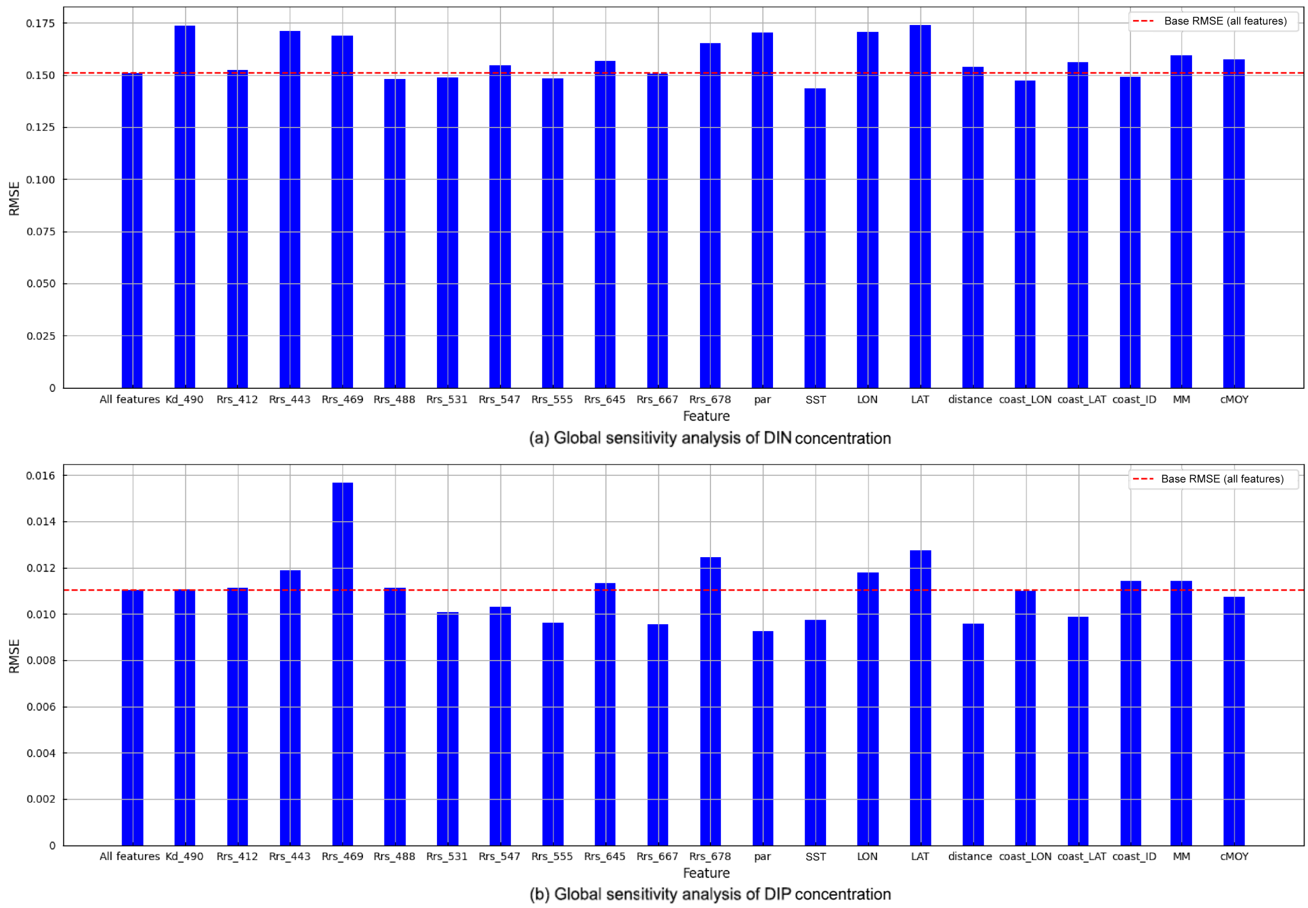

(a) Global sensitivity analysis of DIN concentration

(b) Global sensitivity analysis of DIP concentration

Fig. 9 Global sensitivity analysis bar charts for (a) DIN and (b) DIP concentrations. The bar charts represent the average RMSE of model results after removing a specific feature during model development. The red dashed line indicates the average RMSE of the initial model with all features included.

However, in the retrieval of optically inactive nutrients, such as DIN and DIP, the correlation between remote sensing reflectance and nutrient concentrations is often lower than that with spatiotemporal features. In most satellite-based remote sensing studies, sensor pixel data and *in situ* observations are spatially matched primarily using geographic coordinates (latitude and longitude), making these coordinates critical components of the model inputs. Nonetheless, due to the limited volume of training data, models often fail to capture the spatial continuity of oceanographic variables. As a result, the linear variation of longitude and latitude may introduce substantial artifacts in the final retrieval results, often manifesting visually as cross-shaped striping patterns. Similar artifacts have been observed in the results of other researchers as well[13].

In our study, we innovatively introduced a second coordinate system, using coastal ID and offshore distance to more accurately represent ocean surface locations. Compared with raw geographic coordinates, this alternative coordinate system better captures regional characteristics and exhibits stronger spatial continuity. Moreover, the use of this dual-coordinate system substantially mitigates the cross-shaped striping effects caused by the limitations of using latitude and longitude alone. We present the retrieval results of two models—with and without the inclusion of coastal information—in Fig. 10. In the model that uses only latitude and longitude as spatial input features, noticeable cross-shaped striping noise appears in regions with high nutrient concentrations. After incorporating coastal information into the model input, this noise is significantly reduced, indicating the effectiveness of including coastal context in improving retrieval quality.

4.2 Relationship between nutrient concentration anomalies and climatic factors

We calculated nutrient concentration anomalies for the

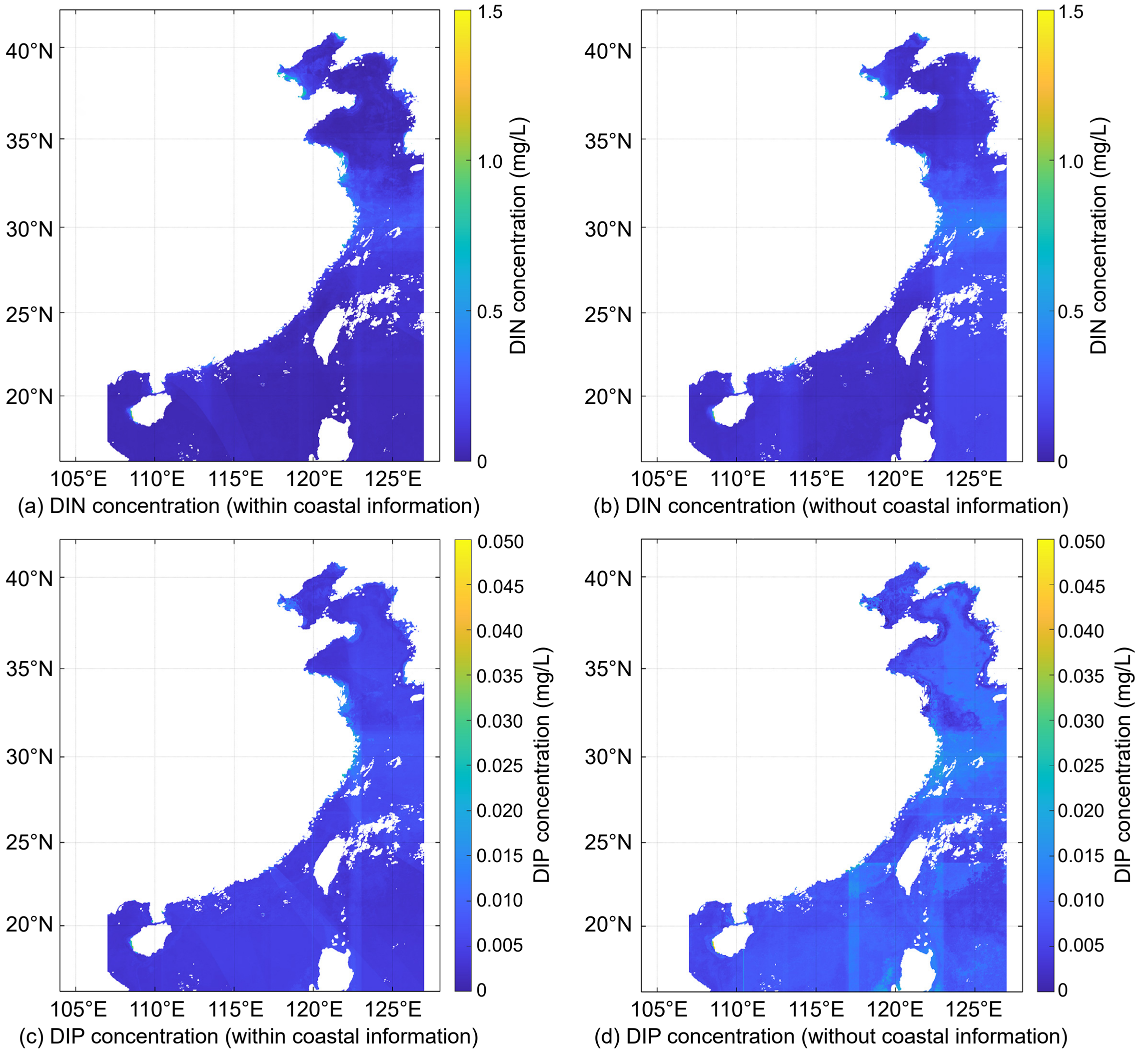

Fig. 10 Performance comparison of different input parameter combinations for remote sensing retrieval of DIN and DIP concentrations. Based on both the availability of valid data and the clarity of contrast in the results, we selected the original outputs from May 2020 as a representative case study. (a) DIN concentration retrieval results with coastal information included; (b) DIN concentration retrieval results without coastal information; (c) DIP concentration retrieval results with coastal information; and (d) DIP concentration retrieval results without coastal information.

three regions and compared them with the Niño 3.4 index anomalies (Fig. 11). The distribution of anomalies suggests that the impact of El Niño or La Niña events on coastal nutrient concentrations exhibits a certain lag. The period from 2014 to 2016 was marked by a strong El Niño event, and in the following year or during the summer of the El Niño year, East Asia often experienced flooding and warmer temperatures. As a result, nutrient concentration anomalies in all regions reached relatively high levels in 2017. In the Changjiang River Estuary–Hangzhou Bay region, the high anomalies in 2020 were lower than those in 2019, and the duration of low anomalies extended by one month. In the Bohai Bay region, increased river discharge from the Yellow River due to warmer temperatures led to a significant rise in high anomalies in 2020 compared to 2019. During La Niña winters, temperatures tend to be lower, resulting in higher-than-usual anomalies in the Bohai Bay and Changjiang River Estuary–Hangzhou Bay regions in 2021. La Niña events are often accompanied by severe winters and droughts, reducing the net flow of the Yangtze and Yellow Rivers and consequently lowering nutrient levels at their estuaries. This explains why the high anomalies in the Bohai Bay and Changjiang River Estuary–Hangzhou Bay regions were lower in 2019 than in 2018. Additionally, the persistent La Niña conditions since August 2020 led to a continuous

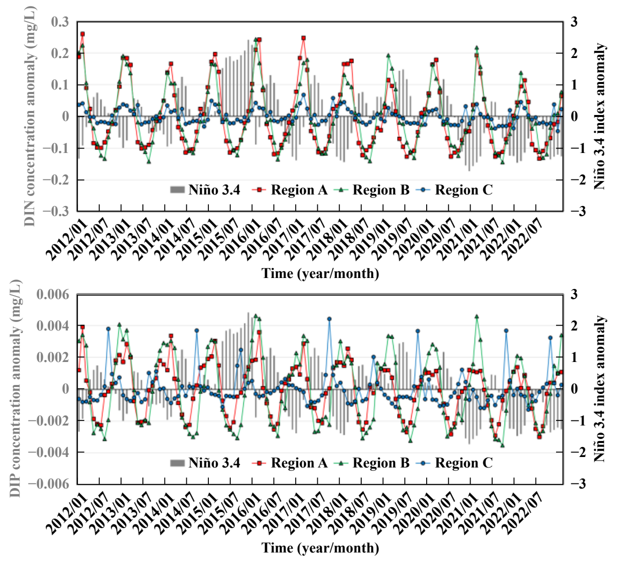

Fig. 11 Comparison of DIN and DIP concentrations retrieval results with and without coastal information in input parameters under otherwise identical conditions. Gray bars represent Niño 3.4 index anomalies.

decline in nutrient concentrations in these regions. In contrast, nutrient anomalies in the Zhujiang River Estuary remained relatively stable, with no significant correlation to the Niño index. We infer that nutrient concentration changes in this region may be less influenced by global climate variability and more affected by human activities.

4.3 Influence of terrestrial environments on coastal nutrient distribution

Nighttime light remote sensing data have been widely used to study economic activities and development at national or regional scales. Generally, changes in nighttime lights show a positive correlation with various indicators of human development. We downloaded monthly averaged VIIRS nighttime light data from 2012 to 2022. For the entire study area, we calculated the Mann–Kendall trend coefficient for each pixel in both nighttime light and nutrient data to assess development levels and nutrient trends across different locations. Additionally, we computed the annual average nighttime light levels for the Bohai Bay, Changjiang River Estuary–Hangzhou Bay, and Zhujiang River Estuary regions for comparative analysis (Fig. 12). The national distribution of nighttime lights clearly shows that areas near major river estuaries exhibit both high light levels and high nutrient concentrations, suggesting that well-developed coastal regions and areas around river mouths are significant sources of coastal nutrient inputs. Among the three key regions, the Bohai Bay area lags behind the Changjiang River Delta and Zhujiang River Delta in terms of both urbanization level and development speed, with the Zhujiang River Delta showing slightly faster development than the Changjiang River Delta. Both DIN and DIP concentrations exhibit similar trends, with nutrient levels decreasing near river estuaries and slightly increasing in offshore areas. This indicates a gradual reduction in terrestrial nutrient inputs in recent years, while the influence of offshore seawater intrusion on coastal nutrient dynamics is expanding. In recent years, China has increasingly prioritized coastal water quality management, implementing a series of policies to control nutrient inputs into the sea. Our findings suggest that these policies have effectively restricted nutrient inputs without hindering urban development.

We extracted annual river discharge and sediment load data for the Yellow River, Changjiang River, and Zhujiang River from 2012 to 2022. The data were sourced from the annual China River Sediment Bulletin, which uses cross-sectional sampling combined with flow measurements to estimate suspended sediment transport rates and derives daily, monthly, and annual sediment loads based on water and sediment processes. As shown in Fig. 13, the Changjiang River Estuary is characterized by high nutrient concentrations and high discharge, while the Yellow River Estuary exhibits high nutrient concentrations and high sediment loads. In contrast, the Zhujiang River Estuary has relatively low river discharge, sediment loads, and nutrient concentrations. Correlation analysis (Table 6) reveals that in the Bohai Bay region, river discharge shows a strong negative correlation with nutrient concentrations, while sediment load has a weak correlation. This suggests that Yellow River water dilutes nutrient concentrations at the estuary, and sediment from the Yellow River is not the primary source of nutrients. Instead, seawater intrusion may be the main driver of nutrient concentration changes in this region. In the Changjiang River Estuary–Hangzhou Bay region, river discharge shows a weak relationship with nutrient concentrations, while sediment load exhibits a stronger correlation. This indicates that riverine inputs are a significant source of nutrients, but the distribution and diffusion of nutrients at the estuary are influenced more by seawater mixing, which drives seasonal nutrient

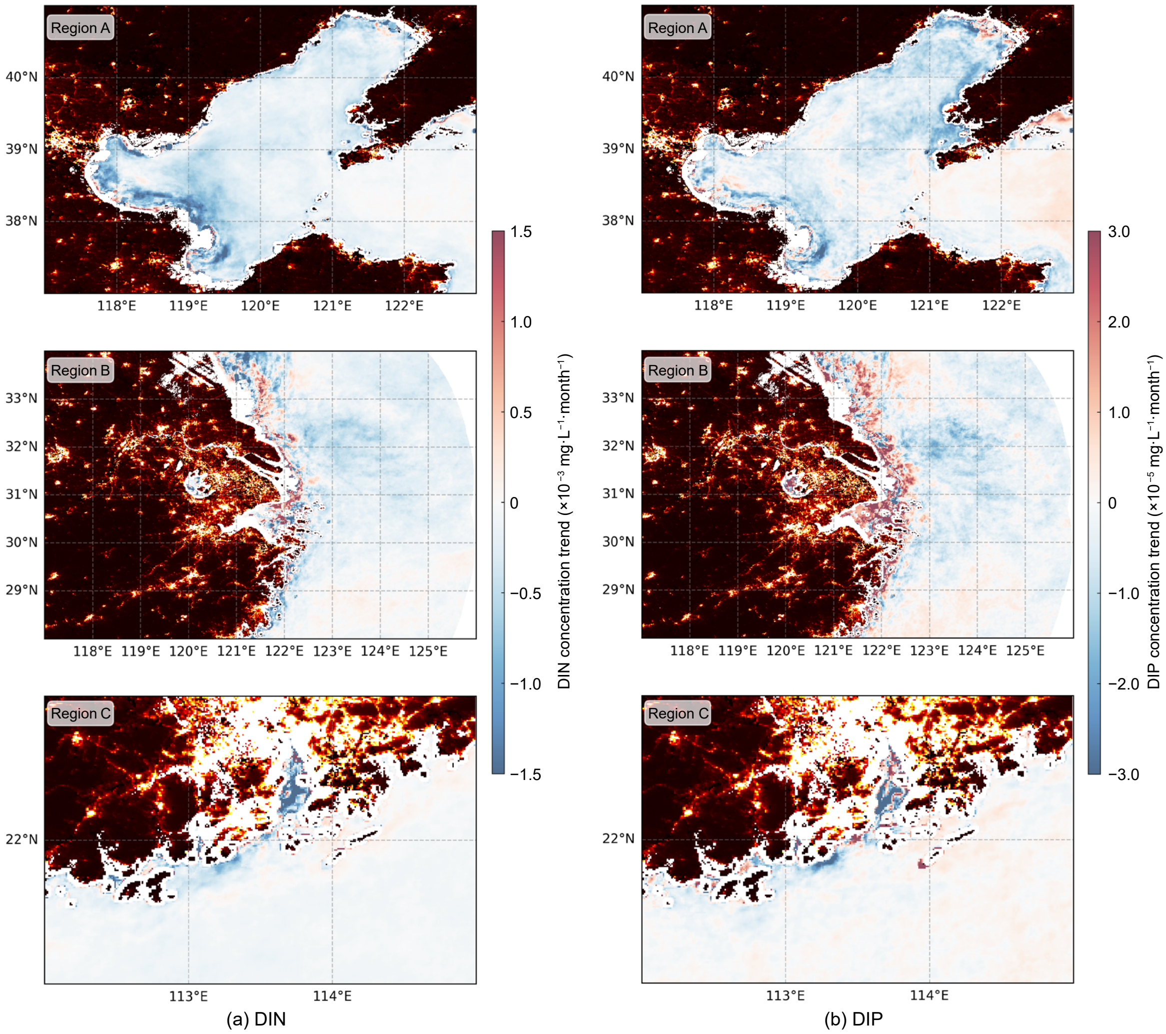

Fig. 12 Spatial distribution of trends in remotely sensed DIN and DIP concentrations across three major study sea areas. Within the sea areas, red and blue pixels represent the slope of monthly average remotely sensed DIN and DIP concentrations calculated using the Mann–Kendall test. Within land areas, pixel brightness represents the trend in nighttime light levels derived from VIIRS nighttime light remote sensing data, with brighter pixels indicating a increase in nighttime light levels.

patterns. In the Zhujiang River Estuary, both river discharge and sediment load show strong positive correlations with nutrient concentrations, highlighting the importance of terrestrial inputs. The similar trends between nutrient concentrations and sediment suggest that a portion of nutrients may enter the sea bound to riverine particles.

We also calculated annual terrestrial precipitation for the three regions and compared it with monthly nutrient concentrations. Overall, the Yellow River Estuary has the lowest precipitation, and similar to river discharge, precipitation shows a strong negative correlation with nutrient concentrations. We hypothesize that precipitation in this region primarily affects river flow, enhancing the dilution effect of Yellow River water on nutrient concentrations. In the Changjiang River Estuary–Hangzhou Bay region, both sediment load and precipitation show strong negative correlations with nutrient concentrations. We speculate that precipitation in this area influences river and estuary nutrient levels and may contribute to sediment resuspension. In the Zhujiang River Estuary, despite high precipitation levels, there is almost no correlation with nutrient concentrations. We infer that precipitation has minimal impact here, and nutrient inputs are primarily sourced from the Zhujiang River.

4.4 Optimization of *in situ* sampling points using remote sensing retrieval results

Remote sensing retrieval results for nutrient concentrations provide additional spatiotemporal perspectives for regional nutrient monitoring. We

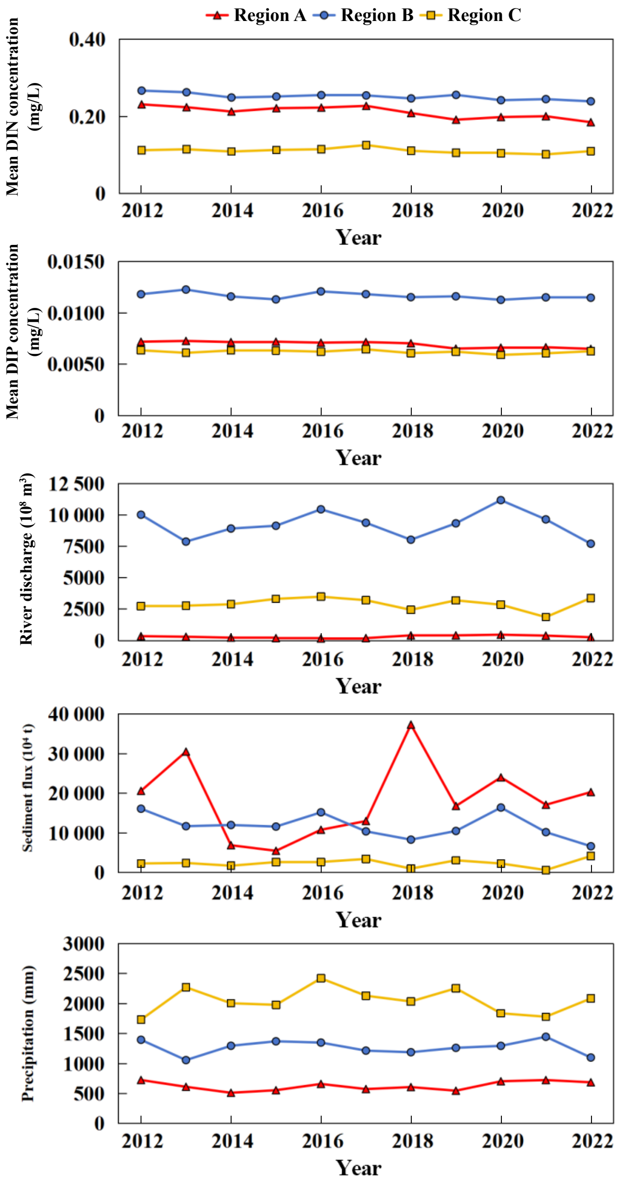

Fig. 13 Line graphs showing annual average trends in nutrient concentrations, river discharge, sediment flux, and precipitation for the three regions. Red triangles represent the Bohai Bay (Region A), blue circles represent the Changjiang River Estuary–Hangzhou Bay (Region B), and yellow rectangles represent the Zhujiang River Estuary (Region C).

explored the supplementary information offered by remote sensing products from both temporal and spatial dimensions.

In situ sampling is typically conducted on a seasonal basis. Therefore, we generated six-year averaged quarterly nutrient distribution maps alongside the distribution of sampling points during the same periods (Fig. 14). In terms of magnitude, nutrient levels in the Bohai Bay and Changjiang River Estuary–Hangzhou Bay regions are generally higher during winter (January–March), particularly in January and February. However, no water quality sampling is conducted during this period, resulting in significant data gaps. Remote sensing retrieval results effectively fill these gaps. For other seasons, remote sensing data also capture monthly variations, ensuring continuous nutrient monitoring throughout the year.

Spatially, only a few sampling points are distributed in open ocean areas, and these are limited to the summer months. Although nutrient levels in open ocean regions are generally negligible, their exclusion from sampling overlooks valuable information. During autumn and winter, nutrients are visibly transported along the East China Sea plume into offshore regions—an effect that is often undetectable through *in situ* sampling alone.

Furthermore, high nutrient concentrations are observed west of Hainan Island and the Leizhou Peninsula, areas not covered by intensive sampling. Seasonal sampling points could be added in these regions to better capture local nutrient dynamics.

In summary, remote sensing results reveal opportunities to optimize the spatial and temporal distribution of *in situ* sampling points. Temporally, *in situ* data cover less than 25% of the year. Spatially, sampling points are concentrated in nearshore areas, with limited coverage of offshore regions, potentially overlooking areas with significant nutrient distributions.

Table 6 Correlation coefficients between nutrient concentrations and river discharge, sediment flux, and precipitation in the three major study areas. Annual average data were used for river discharge and sediment flux, while monthly average data were used for precipitation.

Factor	Correlation coefficient (*r*)					
	Region A		Refion B		Region C	
	DIN concentration	DIP concentration	DIN concentration	DIP concentration	DIN concentration	DIP concentration
Annual river discharge	−0.50	−0.54	0.07	−0.15	0.50	0.50
Annual sediment flux	−0.17	−0.11	0.44	0.19	0.47	0.47
Monthly precipitation	−0.63	−0.53	−0.63	−0.71	−0.40	0.00

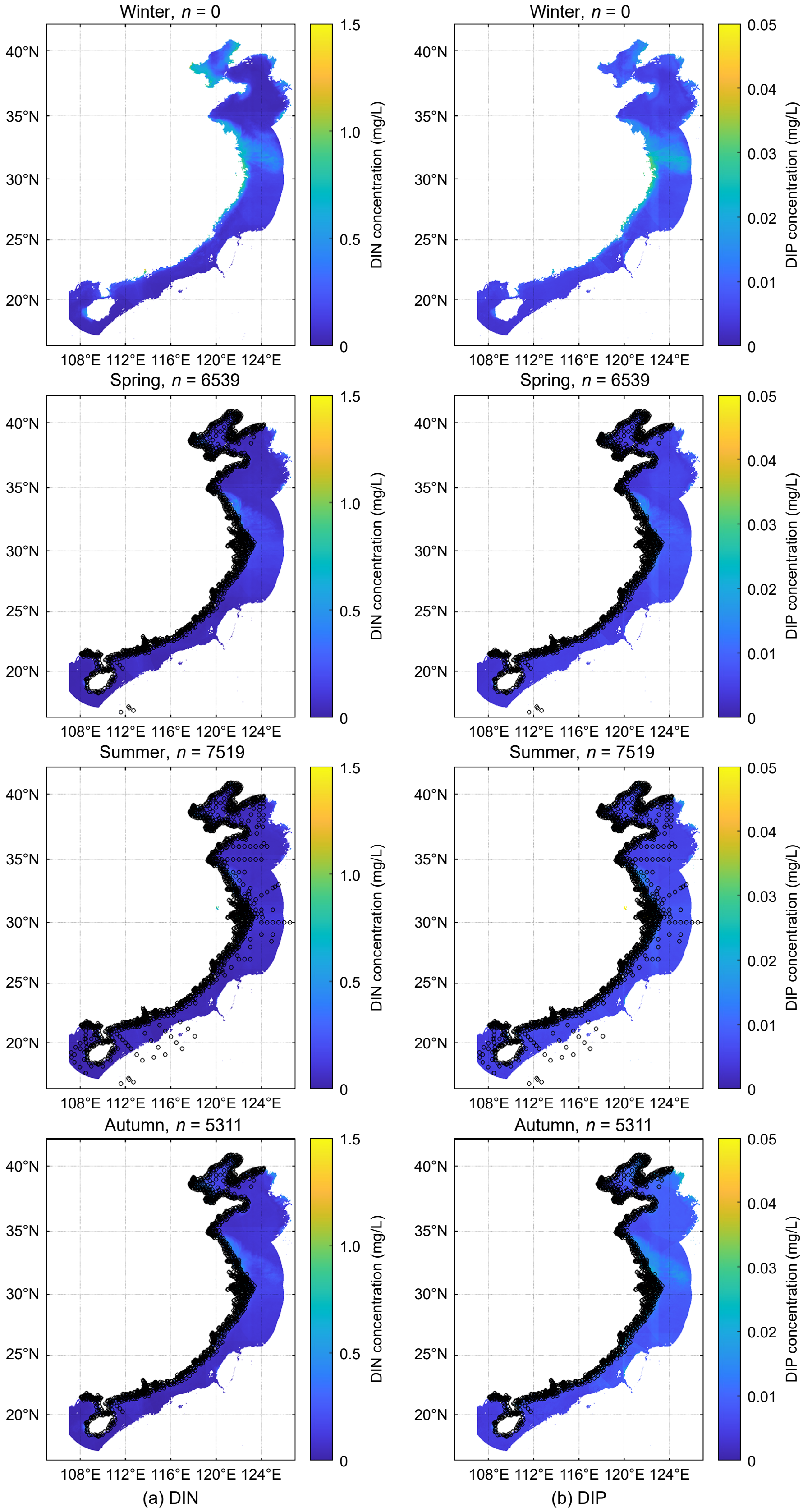

Fig. 14 **Seasonal averaged nutrient concentration distributions and sampling point locations.**

5 Conclusion

This study utilized publicly available *in situ* nutrient datasets to develop retrieval models for DIN and DIP concentrations in China's coastal waters using XGBoost. These models were applied to MODIS satellite data to produce monthly nutrient concentration products from 2012 to 2022.

This research is the first to incorporate a dual-coordinate system in nutrient retrieval for diverse and complex marine environments, significantly improving model accuracy (DIN concentration: R^2 = 0.82, RMSE = 0.09; DIP concentration: R^2 = 0.65, RMSE = 0.006). The introduction of dual coordinates also mitigated the striping effects caused by relying solely on latitude and longitude. Our mesoscale nutrient products provide valuable supplementary information for China's coastal marine environments, addressing spatial gaps in *in situ* sampling and filling data blind spots during winter. Furthermore, the remote sensing retrieval results offer important insights for optimizing the distribution of *in situ* sampling points. The broader perspective provided by remote sensing enables targeted management of nutrient dynamics in different marine regions, supporting national marine environmental monitoring policies.

Based on the retrieval results, we summarize and discuss the following conclusions:

● The average nutrient concentrations in the Bohai Bay and Changjiang River Estuary–Hangzhou Bay regions are higher than those in the Zhujiang River Estuary. Temporally, DIN and DIP concentrations in the Bohai Bay and Changjiang River Estuary–Hangzhou Bay exhibit higher levels in winter and lower levels in summer, while the Zhujiang River Estuary shows the opposite trend, with higher levels in summer and lower levels in winter. Spatially, high nutrient concentrations in the Bohai Bay and Zhujiang River Estuary are confined to their respective estuaries, whereas in the Changjiang River Estuary–Hangzhou Bay, high nutrient levels extend into the western Pacific offshore regions.

● Coastal nutrient distributions are influenced by both riverine inputs and seawater intrusion. In the Bohai Bay, seawater intrusion directly affects nutrient concentrations. In the Changjiang River Estuary–Hangzhou Bay, nutrients from the Changjiang River are transported by ocean currents to other estuaries, influencing nutrient distribution along the coast. In the Zhujiang River Estuary, riverine inputs are the primary nutrient source, with seasonal variations in ocean currents driving nutrient distribution patterns.

● Remote sensing technology complements critical information missing from *in situ* measurements. Temporally, remote sensing fills data gaps during winter and captures monthly variations in nutrient concentrations. Spatially, remote sensing better captures phenomena such as nutrient transport via the East China Sea plume and the influence of coastal currents on nutrient distribution in the Zhujiang River Estuary. These results demonstrate the immense potential of remote sensing for mesoscale nutrient monitoring and provide a new approach for modeling non-optically active parameters in complex marine environments through the incorporation of diverse spatial information.

Acknowledgment

This work was supported by the National Natural Science Foundation of China (Nos. 42476174 and 41476157) and the National Key Research and Development Program of China (Nos. 2018YFB0505005 and 2017YFC1405300).

References

[1] E. T. Harvey, S. Kratzer, and P. Philipson, Satellite-based water quality monitoring for improved spatial and temporal retrieval of chlorophyll-a in coastal waters, *Remote Sens. Environ.*, vol. 158, pp. 417–430, 2015.

[2] D. Liu, S. Yu, and H. Duan, Different storm responses of organic carbon transported to lake Taihu by the eutrophic Tiaoxi River, China, *Sci. Total Environ.*, vol. 782, p. 146874, 2021.

[3] T. C. Malone and A. Newton, The globalization of cultural eutrophication in the coastal Ocean: Causes and consequences, *Front. Mar. Sci.*, vol. 7, p. 760, 2020.

[4] D. M. Anderson, J. M. Burkholder, W. P. Cochlan, P. M. Glibert, C. J. Gobler, C. A. Heil, R. M. Kudela, M. L. Parsons, J. E. J. Rensel, D. W. Townsend, et al., Harmful algal blooms and eutrophication: Examining linkages from selected coastal regions of the United States, *Harmful Algae*, vol. 8, no. 1, pp. 39–53, 2008.

[5] H. W. Paerl, Coastal eutrophication and harmful algal blooms: Importance of atmospheric deposition and groundwater as "new" nitrogen and other nutrient sources, *Limnol. Oceanogr.*, vol. 42, no. 5part2, pp. 1154–1165, 1997.

[6] W. A. Wurtsbaugh, H. W. Paerl, and W. K. Dodds, Nutrients, eutrophication and harmful algal blooms along the freshwater to marine continuum, *WIREs Water*, vol. 6, no. 5, p. e1373, 2019.

[7] G. M. Hallegraeff, A review of harmful algal blooms and

their apparent global increase, *Phycologia*, vol. 32, no. 2, pp. 79–99, 1993.

[8] C. Niu, K. Tan, X. Jia, and X. Wang, Deep learning based regression for optically inactive inland water quality parameter estimation using airborne hyperspectral imagery, *Environ. Pollut.*, vol. 286, p. 117534, 2021.

[9] E. M. Isenstein and M. H. Park, Assessment of nutrient distributions in Lake Champlain using satellite remote sensing, *J. Environ. Sci.*, vol. 26, no. 9, pp. 1831–1836, 2014.

[10] M. S. Islam Khan, N. Islam, J. Uddin, S. Islam, and M. K. Nasir, Water quality prediction and classification based on principal component regression and gradient boosting classifier approach, *J. King Saud Univ. Comput. Inf. Sci.*, vol. 34, no. 8, pp. 4773–4781, 2022.

[11] W. Song, Y. A, Y. Wang, Q. Fang, and R. Tang, Study on remote sensing inversion and temporal-spatial variation of Hulun lake water quality based on machine learning, *J. Contam. Hydrol.*, vol. 260, p. 104282, 2024.

[12] H. Xu, B. Q. Qin, and G. W. Zhu, Nutrient limitation of cyanobacterial growth in different regions of Lake Taihu in summer, (in Chinese), *China Environ. Sci.*, vol. 32, no. 12, pp. 2230–2236, 2012.

[13] L. Zhu, T. Cui, R. A, X. Pan, W. Zhao, J. Xiang, and M. Cao, Robust remote sensing retrieval of key eutrophication indicators in coastal waters based on explainable machine learning, *ISPRS J. Photogramm. Remote Sens.*, vol. 211, pp. 262–280, 2024.

[14] L. Wang, D. Z. Zhao, and J. H. Yang, Nutrients retrieval in the Dayang River Estuary based on HJ-1 satellite remote-sensed imagery, (in Chinese), *China Environ. Sci.*, vol. 32, no. 1, pp. 136–141, 2012.

[15] S. Wu, J. Qi, Z. Yan, F. Lyu, T. Liu, Y. Wang, and Z. Du, Spatiotemporal assessments of nutrients and water quality in coastal areas using remote sensing and a spatiotemporal deep learning model, *Int. J. Appl. Earth Obs. Geoinf.*, vol. 112, p. 102897, 2022.

[16] Y. M. Chen, D. Y. Sun, S. Q. Wang, M. He, Y. Chen, H. L. Zhang, and Y. Zhang, Spatiotemporal variations of nutrients in Jiangsu coastal waters based on GOCI observations, (in Chinese), *Mar. Environ. Sci.*, vol. 43, no. 5, pp. 766–775, 2024.

[17] Z. Zeng, J. Wang, and X. Liao, Global exponential stability of a general class of recurrent neural networks with time-varying delays, *IEEE Trans. Circuits Syst. I Fundam. Theory Appl.*, vol. 50, no. 10, pp. 1353–1358, 2003.

[18] L. Jin, L. Wei, and S. Li, Gradient-based differential neural-solution to time-dependent nonlinear optimization, *IEEE Trans. Autom. Control*, vol. 68, no. 1, pp. 620–627, 2023.

[19] M. Liu, L. Chen, X. Du, L. Jin, and M. Shang, Activated gradients for deep neural networks, *IEEE Trans. Neural Netw. Learn. Syst.*, vol. 34, no. 4, pp. 2156–2168, 2023.

[20] J. Lin, P. Wang, J. Wang, Y. Zhou, X. Zhou, P. Yang, H. Zhang, Y. Cai, and Z. Yang, An extensive spatiotemporal water quality dataset covering four decades (1980–2022) in China, *Earth Syst. Sci. Data*, vol. 16, no. 2, pp. 1137–1149, 2024.

[21] GEBCO Bathymetric Compilation Group 2024, The GEBCO_2024 Grid - a continuous terrain model of the global oceans and land. NERC EDS British Oceanographic Data Centre NOC, https://www.bodc.ac.uk/data/published_data_library/catalogue/10.5285/1c44ce99-0a0d-5f4f-e063-7086abc0ea0f/, 2024.

[22] S. Peng, Y. Ding, W. Liu, and Z. Li, 1 km monthly temperature and precipitation dataset for China from 1901 to 2017, *Earth Syst. Sci. Data*, vol. 11, no. 4, pp. 1931–1946, 2019.

[23] T. Chen and C. Guestrin, XGBoost: A scalable tree boosting system, in *Proc. 22nd ACM SIGKDD Int. Conf. Knowledge Discovery and Data Mining*, San Francisco, CA, USA, 2016, pp. 785−794.

[24] W. J. Moses, S. G. Ackleson, J. W. Hair, C. A. Hostetler, and W. D. Miller, Spatial scales of optical variability in the coastal ocean: Implications for remote sensing and in situ sampling, *J. Geophys. Res. Oceans*, vol. 121, no. 6, pp. 4194–4208, 2016.

[25] B. B. Barnes, J. P. Cannizzaro, D. C. English, and C. Hu, Validation of VIIRS and MODIS reflectance data in coastal and oceanic waters: An assessment of methods, *Remote Sens. Environ.*, vol. 220, pp. 110–123, 2019.

[26] J. M. Beckers and M. Rixen, EOF calculations and data filling from incomplete oceanographic datasets, *J. Atmos. Oceanic Technol.*, vol. 20, no. 12, pp. 1839−1856, 2003.

[27] A. Alvera-Azcárate, A. Barth, M. Rixen, and J. M. Beckers, Reconstruction of incomplete oceanographic data sets using empirical orthogonal functions: Application to the Adriatic Sea surface temperature, *Ocean Model.*, vol. 9, no. 4, pp. 325–346, 2005.

Zhuoqi Zheng received the BS degree in marine technology from Ocean University of China, Qingdao, China, in 2019, the MS degree in physical oceanography from the Second Institute of Oceanography, Ministry of Natural Resources, Hangzhou, China, in 2022. He is currently pursuing the PhD degree at School of Geography and Ocean Science, Nanjing University, Nanjing, China. His research interests mainly focus on the evaluation of waters quality in offshore waters with remote sensing technology.

Zhenke Zhang received the bachelor degree in geography and the master degree in natural geography (geomorphology direction) from Henan University, Zhengzhou, China, in 1985 and 1988, and the PhD degree from the Institute of Geography and Lake Research, Chinese Academy of Sciences, Nanjing, China, in 1998. Currently, he is a doctoral supervisor at Nanjing University, Nanjing, China. His main research direction is African resources and environment.

Delu Pan received the bachelor degree from Nanjing University of Science and Technology, Nanjing, China, in 1968 and then began his career at the 1423 Research Institute of the Commission of Science, Technology and Industry for National Defense. Since 1977, he has been with the Second Institute of Oceanography, State Oceanic Administration (now the Second Institute of Oceanography, Ministry of Natural Resources), Hangzhou, China, where he has focused on ocean remote sensing and held positions as assistant researcher, associate researcher, and researcher. He currently leads the Key Laboratory of Satellite Ocean Dynamics and Environment, the Second Institute of Oceanography, Ministry of Natural Resources, Hangzhou, China. He is an academician of the Chinese Academy of Engineering. He has published over 140 papers and received the National Science and Technology Award in 2003. His research interests include ocean color remote sensing, inversion models, and application technologies.

Fang Gong received the BS degree in computer and application from Nanjing University of Information Science and Technology, Nanjing, China, in 2001. She is currently a senior engineer with the State Key Laboratory of Satellite Ocean Environment Dynamics, the Second Institute of Oceanography, Ministry of Natural Resources, Hangzhou, China. She is also affiliated with the Observation and Research Station for Marine Risk and Hazard Management at Daya Bay, Ministry of Natural Resources, Huizhou, China. Her research interests include satellite data processing and analysis for ocean environment monitoring in the open ocean and nearshore waters.

Xianqiang He received the BS degree in marine and ocean engineering from Huazhong University of Science and Technology, Wuhan, China, in 1999, the MS degree in physical oceanography from the Second Institute of Oceanography, State Oceanic Administration (now the Second Institute of Oceanography, Ministry of Natural Resources), Hangzhou, China, in 2002, and the PhD degree in physical electronics from the Shanghai Institute of Technical Physics, Chinese Academy of Sciences, Shanghai, China, in 2007. He is currently with the State Key Laboratory of Satellite Ocean Environment Dynamics, the Second Institute of Oceanography, Ministry of Natural Resources, Hangzhou, China. He is also currently with Donghai Laboratory, Zhoushan, China, and School of Oceanography, Shanghai Jiao Tong University, Shanghai, China. His research interests include radiative transfer in the coupled ocean and atmosphere system, atmospheric correction of satellite ocean color remote sensing, and oceanography research using ocean color remote sensing data.

Difeng Wang received the BS degree in electronic engineering from Xiamen University, Xiamen, China, in 2001, the MS degree in physical oceanography from the Second Institute of Oceanography, State Oceanic Administration (now the Second Institute of Oceanography, Ministry of Natural Resources), Hangzhou, China, in 2004, and the PhD degree in electromagnetic fields and microwave techniques from the Graduate School of Chinese Academy of Sciences, Shanghai, China, in 2010. He is currently a research scientist of remote sensing at the State Key Laboratory of Satellite Ocean Environment Dynamics, the Second Institute of Oceanography, Ministry of Natural Resources, Hangzhou, China. He is also affiliated with the Observation and Research Station for Marine Risk and Hazard Management at Daya Bay, Ministry of Natural Resources, Huizhou, China. His research interests include ocean environment and water quality monitoring via satellites, including chlorophyll, nutrients, and suspended sediment in the open ocean and nearshore waters.

Jingjing Huang received the BS degree in marine technology from Nanjing University of Information Science and Technology, Nanjing, China, in 2019 and received the MS degree in physical oceanography from the Second Institute of Oceanography, Ministry of Natural Resources, Hangzhou, China, in 2022. She is currently a joint PhD student at Ocean College, Zhejiang University, Zhoushan, China, and the Second Institute of Oceanography, Ministry of Natural Resources, Hangzhou, China. Her research interests include the estimation of nutrient concentrations in offshore waters with remote sensing technology.

Qing Zhang received the BS degree in marine technology from Shanghai Ocean University, Shanghai, China, in 2022. She is currently pursuing the MS degree in physical oceanography at the Second Institute of Oceanography, Ministry of Natural Resources, Hangzhou, China. Her research interests include ocean remote sensing data fusion and applications.

Aifen Zhong received the BS degree in marine technology from Shanghai Ocean University, Shanghai, China, in 2023. She is currently pursuing the MS degree in physical oceanography at the Second Institute of Oceanography, Ministry of Natural Resources, Hangzhou, China. Her research interests include the estimation of global sea surface nutrient concentrations with remote sensing technology.